Reactivity towards oxygen and cation distribution of manganese iron spinel $Mn_{3-x}Fe_xO_4$ ($0 \leqslant x \leqslant 3$) fine powders studied by thermogravimetry and IR spectroscopy

Bernard Gillot,*[a] Moha Laarj[b] and Sadi Kacim[b]

[a]*Laboratoire de Recherches sur la réactivité des solides, UMR 5613, Faculté des Sciences Mirande, B.P. 138, 21004 Dijon Cedex, France*

[b]*Département de Chimie, Faculté des Sciences Semlalia, B.P.S. 15, Marrakech, Morocco*

The thermal behaviour in oxygen and the cation distribution of manganese iron spinels $Mn_{3-x}Fe_xO_4$ ($0 \leqslant x \leqslant 3$) obtained by a soft chemistry method have been determined by thermogravimetry and IR spectroscopy . The existence of two different cation distributions as function of composition x is established from a quantitative analysis by derivative thermogravimetry. For $x > 1.50$, the IR spectroscopy clearly distinguished the presence of Fe^{2+} and Mn^{2+} ions located in octahedral and tetrahedral sites, respectively. For $x < 1.50$, this method is also efficient for the differentiation of the Mn^{2+} ions located in both types of site of the spinel structure. Kinetic studies on the oxidation process of Mn^{2+} ions show that the oxidation proceeds by way of a diffusion-controlled reaction or by a nucleation–growth mechanism. The difference in the kinetic behaviour is interpreted with regard to a structural change from the cation-deficient spinel to multi-phase oxides initiated by the oxidation temperature.

Manganese–iron oxides $Mn_{3-x}Fe_xO_4$ with spinel structures ($0 \leqslant x \leqslant 3$) have been studied extensively. Manganese ferrites ($x > 1.50$) are used widely in electronics, and their magnetic and electrical properties[1–3] are affected strongly by the method of preparation. For iron manganites ($x < 1.50$), most studies have concentrated on the determination of crystallographic properties, *i.e.* distortion of the normally cubic symmetry due to the Jahn–Teller effect.[4] In recent years high-performance negative temperature coefficient thermistors, based on Mn spinels with a high manganese content have been developed.[5,6] More recently, additional interest in Mn–Fe–O systems has developed because of their reportedly improved performance as catalysts in Fischer–Tropsh synthesis.[7,8]

However, for the interpretation of the magnetic, electrical, structural and catalytic properties, knowledge of the distribution and valencies of various cations like Mn^{2+}, Mn^{3+}, Mn^{4+}, Fe^{2+}, Fe^{3+} between the available octahedral (B) and tetrahedral (A) sites is of great importance. In connection with this, the non-stoichiometry of oxygen[9] described as $Mn_{3-x}Fe_xO_{4+\delta}$ with $\delta > 0$ (while an equivalent number of cation vacancies is present) is influenced markedly by the preparation conditions, such as ceramic or soft chemistry routes. Thus in determining the solid phases present in the system Fe_2O_3–Mn_2O_3–O_2 at equilibrium in air above 900 °C, Wickham[10] described the chemical composition of the mixed spinels of iron and manganese and proposed the formula $Mn_{3-x}Fe_xO_{4+\delta}$ with $0 < \delta < 0.04$. For samples prepared *via* the usual ceramic route, Krupicka and Zaveta[11] studied the magnetic and electrical properties of $MnFe_2O_{4+\delta}$ ferrites with a graduated oxygen content, δ, varying from 0 to 0.23. However, their oxidation requires such a high temperature that the spinel structure is usually transformed to a rhombohedral structure.

We have shown in previous papers[12,13] that it is possible to obtain cation-deficient spinels without the formation of other phases and with a larger number of vacancies ($\delta = 0.6$) by the oxidation at low temperature of fine-grained stoichiometric Mn ferrites prepared by soft chemistry. More recently, Jimenez *et al.*[14] have also obtained highly dispersed spinel oxides in the Mn–Fe–O system with a high content of vacancies from the decomposition at low temperature of mixed carbonates. It appears that for stoichiometric spinels the distribution of cations in $Mn_{3-x}Fe_xO_4$ ($0 \leqslant x \leqslant 3$) can be described approximately by three single formulae:

$$(Mn^{2+}_{2.4-0.8x}Fe^{3+}_{0.8x-1.4})_A(Fe^{3+}_{2.8-0.6x}Fe^{2+}_{0.8x-1.4}Mn^{3+}_{0.6-0.2x})_BO_4^{2-} \quad (1)$$

if x is between three and two,[15–17] and for $x < 2$ the distribution of cations has been assumed to be[6,10,17]

$$(Mn^{2+})_A(Fe^{3+}_{3-x}Mn^{3+}_{x-1})_BO_4^{2-} \quad (2)$$

and

$$(Mn^{2+}_{1-y}Fe^{3+}_y)_A(Fe^{3+}_zMn^{3+}_{2-x}Mn^{2+}_y)_BO_4^{2-} \ (x = y + z) \quad (3)$$

In these conditions, as x decreases from three to two, we can consider that the manganese atom enters the structure as Mn^{2+} ions on tetrahedral sites replacing Fe^{2+} ions located on B sites. For $x < 1.50$, the substitution of iron ions by manganese ions leads to the replacement of Fe^{3+} ions by Mn^{2+} and Mn^{3+} ions on B sites, although Mn^{2+} ions, however, prefer tetrahedral cocoordination. In this latter distribution and using quantitative Mössbauer results,[6] the values of the coefficients x, y and z have been calculated.

In this paper, we report an investigation by derivative thermogravimetry (DTG) of the cation distribution in fine powders of the whole system Mn_3O_4–Fe_3O_4 where the two cations manganese and iron can be oxidized successively at low temperature. This method, which is based on the difference in reactivity towards oxygen of iron and manganese ions in relation to occupied sites, is especially suited to this purpose due to the fact that it is possible to carry out a systematic study of the oxidation process in regard to the nature, charge and position of cations in the spinel lattice.[18] The results are compared and evaluated with the previous cation distributions established for the systems Fe_3O_4–$MnFe_2O_4$[12] and Mn_3O_4–Mn_2FeO_4.[19] IR spectroscopic measurements were also investigated for stoichiometric and oxidative non-stoichiometric samples in order to obtain information about the presence of an ordered distribution between cations and vacancies.

Samples and Experimental procedure

Samples

For $x \geqslant 2$, the samples were prepared from the thermal decomposition of mixed iron and manganese oxalates

$(Fe_xMn_{3-x})C_2O_4{\cdot}2H_2O$ ($3 \leqslant x \leqslant 2$) and treated at low temperature in an H_2–H_2O atmosphere in accordance with the conditions stated in ref. 20. Powders of $Mn_{3-x}Fe_xO_4$ were obtained for the following values of iron concentrations: $x = 2.86$, 2.73, 2.63, 2.50, 2.28 and 2. X-Ray diffraction studies showed that the samples had a very pure cubic spinel structure and did not contain manganese oxide, MnO. The particles were roughly spherical with diameters of *ca.* 70 nm.

For $x < 2$ iron manganite spinel powders of different compositions were prepared by the continuous coprecipitation of formate precursors $(Fe_yMn_{1-y})(CHO_2)_2{\cdot}2H_2O$ ($x = 3y$, $0 < x < 2$) following the method described in detail in ref. 6. After thermal decomposition of the formate precursors for 4 h at 1000 °C and quenching to room temperature, some particular compositions, $x = 1.80$, 1.50, 1.30, 1.05, 0.78, 0.58, 0.39, 0.12 and 0, with the desired spinel structure were obtained. According to a scanning electron microscopy study, the particle size was found to be consistent, with grain sizes of *ca.* 7 μm. For samples ground for 10 min, the grain size was *ca.* 300 nm; this allows their partial oxidation to cation-deficient spinels.[21]

Experimental procedure

The oxidations were performed with the temperature increasing linearly (2.5 °C min^{-1}) or under isothermal conditions in a Setaram MTB 10-8 microbalance (symmetrical set-up, resolution and noise level 0.1 μg) using 20 mg of powder. The degree of oxidation at various levels of reaction was calculated from the gravimetry data. FTIR spectra were recorded in air at room temperature with a Perkin-Elmer 1725X instrument over the range 4000–450 cm^{-1} and with a Perkin-Elmer 1700 instrument over the range 450–50 cm^{-1}. Transmittance spectra were realized on 1 mg of powdered sample dispersed in 200 mg of CsI pellets pressed under vacuum at 10 Pa. X-Ray diffraction (XRD) was used to determine the phase purity and crystallographic lattice constants of the samples. All materials were found to be single phase. XRD analyses were performed using a Rigaku 18 kW rotating anode diffraction system equipped with a Cu-target anode. α-Quartz was used as an external calibration standard. For the precise determination of the lattice parameters the X-ray reflections in the range $\theta = 20$–50° were recorded by step scanning, using increments of 0.01° θ and a fixed counting time of 60 s $step^{-1}$. The error in the measured lattice parameter resulting from sample positioning and instrument precision is estimated to be ± 0.0003 nm.

Results and Discussion

Unoxidized samples

In the investigated region (900–100 cm^{-1}) the spectra of samples with $x = 2.86$–2.28 (Fig. 1) reveal two absorption bands ν_1 and ν_2 in good agreement with the spectrum of Fe_3O_4 which also shows two bands at 575 and 360 cm^{-1}.[22] The lower frequency bands observed in the region from 500 to 300 cm^{-1} in these specimens split into two or more components in those of the $x = 2$–0.58 samples (Fig. 1). In addition, in the spectra of $x = 1.30$–0.39 samples, another weak absorption band at *ca.* 170 cm^{-1} was observed. Of these observed bands, the highest one (ν_1) shifts by 23 cm^{-1} to the lower-frequency side from $x = 2$ to 0.58 (Fig. 2). The ν_2 absorption band shows little change from $x = 2.86$ to $x = 1.50$. The measurements of the lattice parameter, *a*, show that the lattice parameter increases from $x = 2.86$ to 2 and then vary little from $x = 2$ to 1.30 (Fig. 2). It has been reported that on moving from $x = 3$ to 2, the (M—O) bond lengths of the A site increase by 0.012 nm, while those of B sites remain nearly constant at *ca.* 0.205 nm.[23] This indicates that the lower-frequency shifts of the ν_1 band in this composition range are associated with the decrease in the bond-stretching force constant of the A sites, which is exhibited in the increase of bond length of the A sites. For $x < 1.05$, the

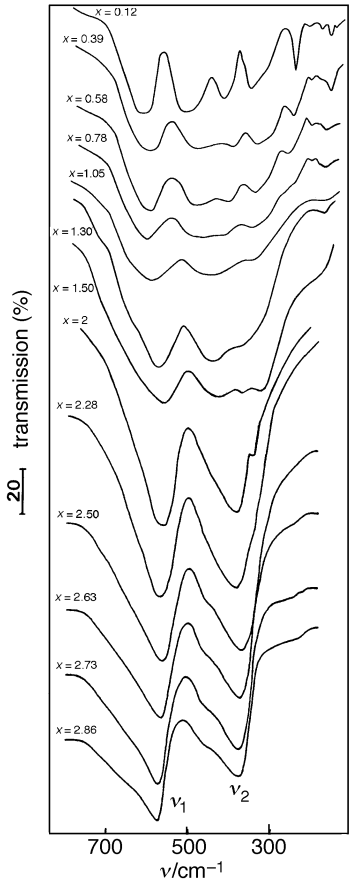

Fig. 1 FTIR spectra for the spinel series $Mn_{3-x}Fe_xO_4$

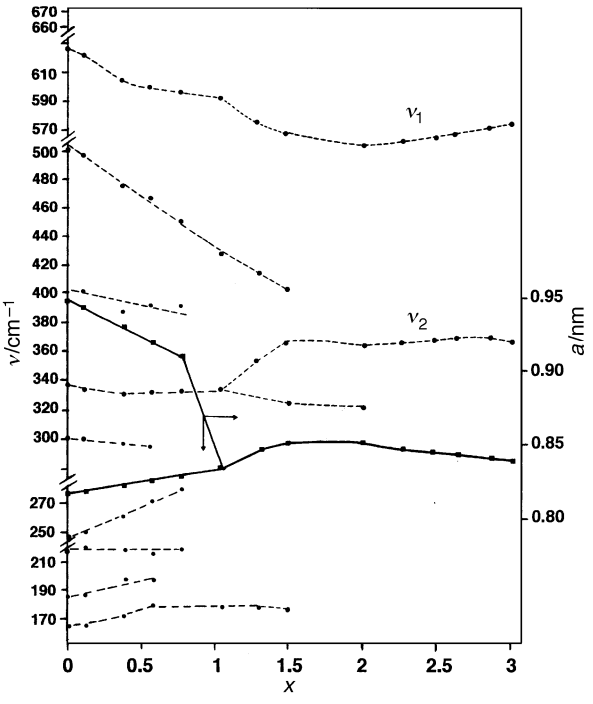

Fig. 2 Compositional dependence of lattice parameter and IR absorption bands for the spinel series $Mn_{3-x}Fe_xO_4$

structural investigation by XRD analysis and FTIR spectroscopy (Fig. 2) reveals a single phase with a distorted tetragonal structure. The observed bands are a premonitory representation of the spectra of tetragonal Mn_3O_4[24] and are due to the nearly localized vibrations of the tetragonally

distorted regions. However, for the intermediary region, $x=2$–1, although the measurements of the lattice constant indicated that the spinels still exhibited the cubic lattice (Fig. 2), some weak absorption bands or shoulders observed in this composition range predicted a transition region. We can postulate that the locally distorted octahedra are distributed randomly in the lattice of cubic $Mn_{3-x}Fe_xO_4$ prior to the transition of the tetragonal phase due to the cooperative interaction of these distorted octahedra.[24]

Oxidized samples

Non-isothermal oxidation. *Cation distribution.* The curves of the derivative mass gain–temperature (DTG curves) show that the reaction consists, except for the $x=0$ and $x=3$ samples, of some distinct oxido-reduction processes (Fig. 3). For $x>1.50$, four oxidation peaks and one reduction peak can be seen clearly after desummation. As already stated, for $x\geqslant 2$ and for fine powders, the three oxidation peaks below *ca.* 500 °C where the spinel structure was maintained[12] can be attributed to the oxidation of Fe^{2+}, Mn^{3+} and Mn^{2+} ions, the difference in the oxidation temperature being due to the difference in the cation–oxygen distances for iron and manganese ions.[18] At higher temperatures, Mn^{4+} ions formed below 500 °C were reduced to Mn^{3+} ions and the unoxidized Mn^{2+} ions were finally completely oxidized to Mn^{3+} ions. This further oxidation is followed by a lattice transformation from a spinel structure to a rhombohedral one in which all the cations are trivalent. A quantitative analysis from the DTG peak areas suggests a cation distribution identical to eqn. (1), which is for $x=2$, similar to the distribution proposed by Hastings and Corliss.[15] This distribution predicts that the Fe^{2+} content is cancelled out for $x=1.75$ which agrees with the low conductivity observed for $x=1.50$.

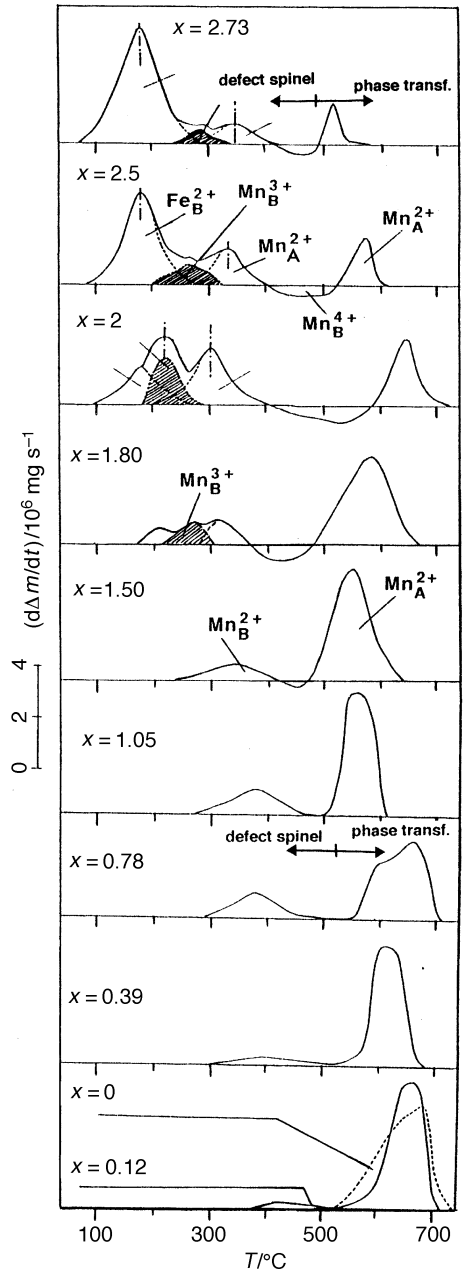

Fig. 3 DTG curves showing the different oxidation stages for $Mn_{3-x}Fe_xO_4$ spinels

In contrast, for $x\leqslant 1.50$, only two oxidation peaks are present in the DTG curves (Fig. 3) with a total mass gain nearly equal for all samples. It has been demonstrated[25] that for an Mn_3O_4 spinel ($x=0$) of cation distribution $(Mn^{2+})_A(Mn^{3+}Mn^{3+})_BO_4^{2-}$, oxidative transformation in air is detectable by a mass gain of 3.48% according to: $Mn_3O_4+1/2O_2\rightarrow 3/2\alpha\text{-}Mn_2O_3$. This seems to be evidence, in opposition to results obtained for samples with $x>1.50$, for the non-oxidation of Mn^{3+} ions. This difference in the behaviour of Mn^{3+} ions may be related to the crystallite size that differs with the preparation method, as mentioned above. For fine-grained samples, the instability of Mn^{4+} ion containing oxide systems has been proved, *e.g.* MnO_2 is completely decomposed in $\alpha\text{-}Mn_2O_3$ at 450 °C in air.[26] In this case the reduction step was thus suppressed. Also, following the absence of Fe^{2+} ions[6] and for the imposed conditions here, the oxidation is solely due to Mn^{2+} ions. Since the sum of the two peak areas nearly corresponds to the peak area measured for the oxidation of Mn_3O_4, we can postulate that for Fe-containing spinels the number of Mn^{2+} ions is almost constant and may be associated with the presence of one Mn^{2+} ion per formula unit. It has been established previously[18] that the oxidation temperature for B-site M^{n+} ions is lower than that for A-site M^{n+} ions because of the weaker ionic bonding of the B sites as compared with the stronger A-site covalent bonds. From this consideration, the two stages of oxidation revealed by the DTG curves would be associated with the oxidation of Mn^{2+} ions from predominantly B and A sites, respectively. A comparison may be made with Mn_3O_4 spinel, where the Mn^{2+} ions originate exclusively on one site. The amount of divalent manganese present on each site can be calculated from the area of the DTG peaks. The cation distribution for this composition range can be described by the formula:

$$(Mn^{2+}_{1-y}Fe^{3+}_y)_A(Fe^{3+}_zMn^{3+}_{2-x}Mn^{2+}_y)_BO^{2-}_4 \quad (x=y+z) \qquad (4)$$

The results obtained make it possible to estimate, with some certainty, the cation distribution in the system $Mn_{3-x}Fe_xO_4$. This distribution is shown in Fig. 4

FTIR study. In Fig. 5, FTIR spectra recorded for samples heated at 450 °C for 1 h (and therefore oxidized) for cation-deficient spinels are shown. For $x\geqslant 2$ and in contrast to unoxidized samples (Fig. 1), the spectra exhibit a large number of absorption bands, those for $x>2.50$ being well resolved. The similarity to the FTIR spectrum of ordered $\gamma\text{-}Fe_2O_3$,[22] both in the position and the number (at least 20) of absorption bands allows us to postulate the same type of order between vacancies and cations on B sites, *i.e.* a □ : cation ratio of 1 : 5. With decreasing x ($2.50>x>2$) and although the number of vacancies per mole increases slightly,[27] numerous absorption bands remain visible as shoulders of vanishing bands. For these defect phases, the vacancies are located on the B sites and result not only from the oxidation of iron ions but also from the oxidation of manganese ones, as indicated in Fig. 3. Spectra recorded for $x\leqslant 1.50$ samples and resulting from the

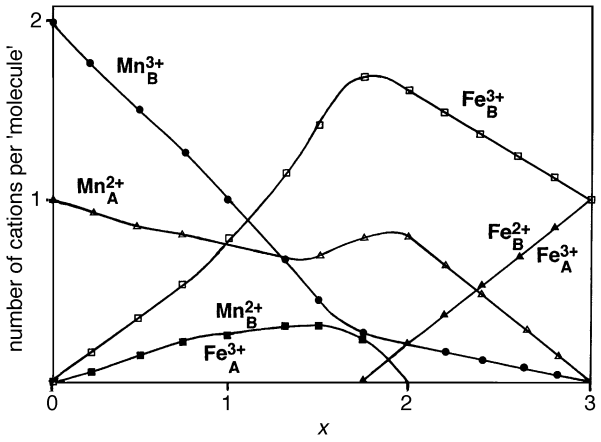

Fig. 4 Compositional dependence of site occupancy fraction for the $Mn_{3-x}Fe_xO_4$ spinels

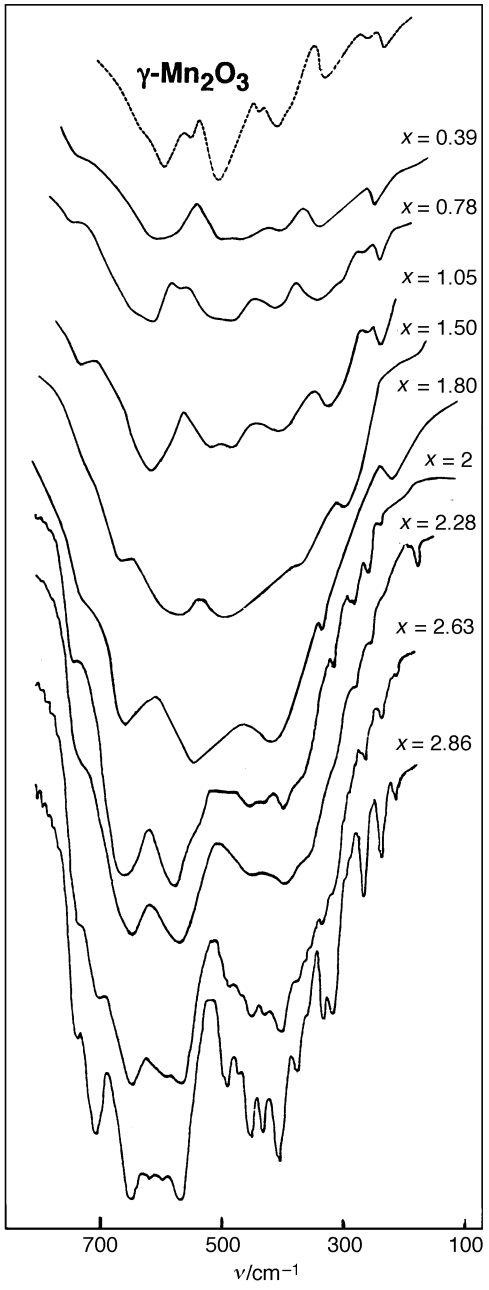

Fig. 5 FTIR spectra of oxidized samples at 450 °C in cation-deficient spinels $Mn_{3-x}Fe_xO_{4+\delta}$

oxidation of Mn_B^{2+} are similar to that presented for γ-Mn_2O_3, although the number of vacancies must be lower because of an incomplete oxidation of manganese ions. For $x \leqslant 1$, in comparison with an initial sample (Fig. 1), the principal intense bands, characteristic of a spinel phase with a distorted tetragonal structure, are better resolved. This results in a greater amount of Mn^{3+} ions in B sites, and consequently in Mn_B^{2+} oxidation which increases the tetragonal distortion. Above 500 °C, the X-ray diffraction pattern and FTIR spectrum indicate that the defect phase tends to transform, as a consequence of the oxidation of Mn_A^{2+}, into a mixture of two phases identified as α-Fe_2O_3 and α-Mn_2O_3 to the corundum structure for $x \leqslant 1.50$ and as α-Mn_2O_3 and cubic $FeMnO_3$ for $x > 1.50$.

Isothermal oxidation: kinetic study. Since the heat-treatment in oxygen leads to a structural change, it is useful to investigate the kinetic behaviour when the oxidation is achieved on the one hand below 450 °C through the formation of the defect spinel phase, and on the other hand above 550 °C with a phase transformation. For this purpose, we considered only the oxidation of Mn^{2+} ions that imply for the compositional range $3 > x > 1.50$ the preliminary oxidation of Fe^{2+} and Mn^{3+} ions. The selected treatment consists of heating under air at 160 °C for 10 h. Note that oxidation without any phase change is due to Mn_B^{2+} ions for $x \geqslant 1.50$ and to Mn_A^{2+} ions for lower iron contents, whereas the oxidation with a phase transformation solely concerned the Mn_A^{2+} ions.

The oxidation kinetics curves, determined as a function of temperature, have a roughly parabolic shape for the oxidation without phase change (Fig. 6 and 7) and a sigmoïdal shape for

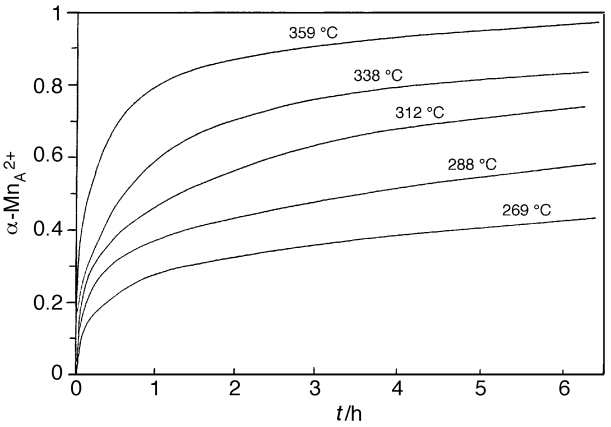

Fig. 6 Kinetic curves $\alpha_A = f(t)$ for tetrahedral Mn^{2+} ions oxidation for a spinel with $x = 2$ ($T < 450$ °C)

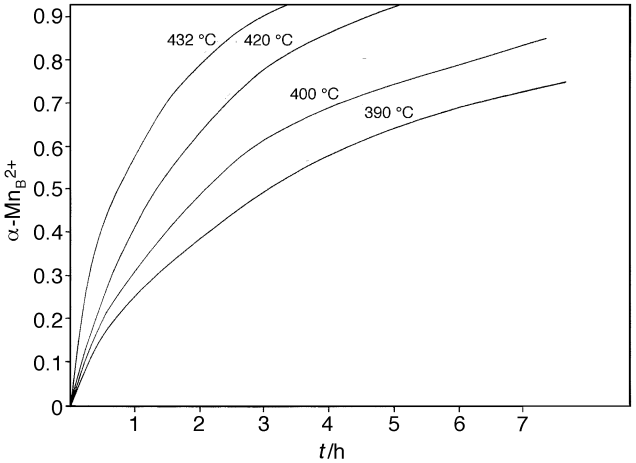

Fig. 7 Kinetic curves $\alpha_B = f(t)$ for octahedral Mn^{2+} ions oxidation for a spinel with $x = 0.78$ ($T < 450$ °C)

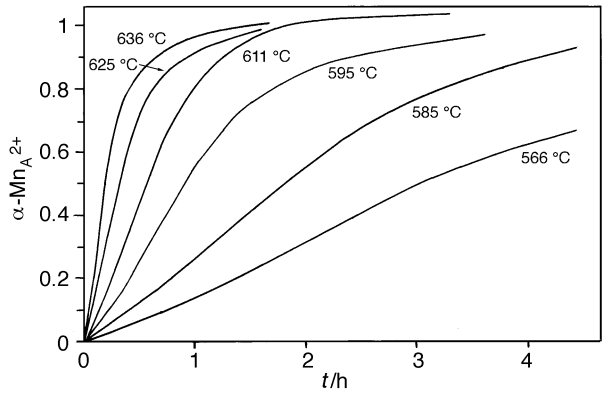

Fig. 8 Kinetic curves $\alpha_A = f(t)$ for tetrahedral Mn^{2+} ions oxidation for a spinel with $x = 2$ ($T > 600$ °C)

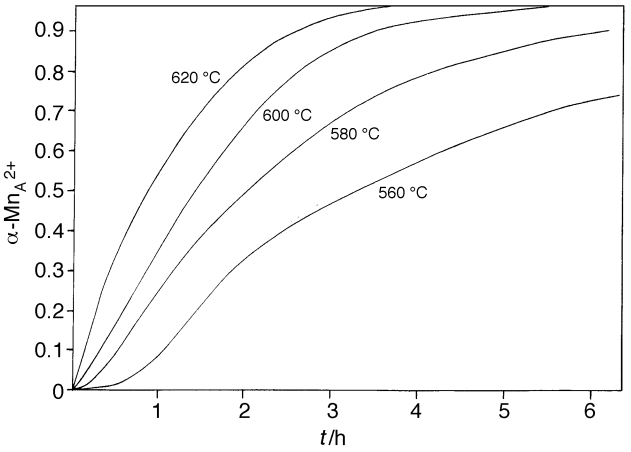

Fig. 9 Kinetic curves $\alpha_A = f(t)$ for tetrahedral Mn^{2+} ions oxidation for a spinel with $x = 0.78$ ($T > 600$ °C)

the oxidation with a phase change (Fig. 8 and 9). In each case the curves can be superimposed,[28] which implies that the controlling process of the reaction is unique and unchanging over the whole considered reaction. The rate law can be expressed in the form of a separate variables expression:

$$v = \mathrm{d}\alpha/\mathrm{d}t = f(\alpha)g(P)h(T) = K_p K_T f(\alpha) P^n \exp(-E/RT) \quad (5)$$

where $f(\alpha)$ is a morphological term characteristic of the reaction area.

At constant temperature and pressure the shape of the curves is determined only by geometrical factors. The conversion rate is defined as α_B and $\alpha_A = W_t/W_\infty$, where W_t is the amount of Mn^{2+} ions oxidized to Mn^{3+} ions at B or A sites in time t, and W_∞ is the corresponding amount after infinite time. For the first oxidation process where the spinel structure was maintained, we have shown that such oxidation can be described as a vacancy diffusion-controlled process obeying the usual Fick's equation with a concentration given at the surface by thermodynamic conditions.[29] The kinetic law, where $F(\alpha)$ is the integrated form of $f(\alpha)$, can be described by the equation:

$$F(\alpha) = \log(1 - \alpha_{A/B}) = A - kt = f(t) \quad (6)$$

where $k = \pi^2 \tilde{D}/r^2$ and $\tilde{D}$ and r are the chemical diffusion coefficient and the mean grain radius, respectively, and A is a constant. A plot of $-\log(1-\alpha_{A/B})$ *vs.* t gives a straight line for $0.2 < \alpha_{A/B} < 0.9$. The activation energy from a plot of $\log \tilde{D}$ *vs.* $1/T$ was 135 kJ mol^{-1} for $x = 2$ and 116.5 kJ mol^{-1} for $x = 0.78$.

For the second oxidation process with phase transformation, the sigmoïdal shape of the reaction is clearly visible and no initial period can be found at the main process. The isotherms were best fitted with the equation:

$$F(\alpha) = 1 - (1 - \alpha_A)^{1/3} = kt \quad (7)$$

Such curves are usually explained on the basis of rapid nucleation but no uniform probability 'contracting envelope' with isotropic growth.[30] An Arrhenius plot of the constant k *vs.* $1/T$ gives for $x = 2$ an activation energy of 230 kJ mol^{-1} and for $x = 0.78$ an energy of only 108 kJ mol^{-1}. For Mn_3O_4 oxidation, an activation energy of 110 kJ mol^{-1} has been reported.

In summary, thermogravimetry and FTIR spectroscopy studies have demonstrated that a change in the cation distribution takes place at $x \approx 1.50$. Also, it appears that the composite nature of the oxidation kinetics can be explained on the basis of the possibility for the same oxidizable cation (Mn^{2+}) to be oxidized in two stages in a large temperature range.

References

1 K. Naito, H. Inaba and H. Yagi, *J. Solid State Chem.*, 1981, **36**, 28.
2 M. Petrera, A. Gennero and N. Burriesci, *J. Mater. Sci.*, 1982, **17**, 429.
3 Ph. Tailhades, A. Rousset, R. Bendaoud, A. Fert and B. Gillot, *Mater. Chem. Phys.*, 1987, **17**, 521.
4 M. O'Keeffe, *J. Phys. Chem. Solids*, 1961, **21**, 172.
5 J. Töpfer, L. Neupert, D. Schütze and P. Wartewig, *J. Alloys Compd.*, 1994, 215, **97**.
6 T. Battault, R. Legros and A. Rousset, *J. Eur. Ceram. Soc.*, 1995, **15**, 1141.
7 G. C. Maiti, R. Malessa, U. Lochner, H. Papp and M. Baerns, *Appl. Catal.*, 1985, **16**, 215.
8 I. R. Leith and M. G. Howden, *Appl. Catal.*, 1988, **37**, 75.
9 K. Kleinstück, E. Wieser, P. Kleinert and R. Perthel, *Phys. Status Solidi*, 1965, **8**, 271.
10 D. G. Wickham, *J. Inorg. Nucl. Chem.*, 1969, **31**, 313.
11 S. Krupicka and K. Zaveta, *Czech. J. Phys.*, 1959, **9**, 324.
12 B. Gillot, M. El Guendouzi, P. Tailhades and A. Rousset, *React. Solids*, 1986, **1**, 139.
13 B. Gillot, M. El Guendouzi and A. Rousset, *J. Solid State Chem.*, 1987, **68**, 285.
14 J. M. Jimenez Mateos, W. Jones, J. Morales and J. L. Tirado, *J. Solid State Chem.*, 1991, **93**, 443.
15 J. M. Hastings and L. M. Corliss, *Phys. Rev.*, 1956, **104**, 328.
16 G. D. Rieck and F. C. M. Dtiessens, *Acta Crystallogr.*, 1966, **20**, 521.
17 A. D. Pelton, H. Schmalzried and J. Sticher, *Ber. Bunsen-Ges. Phys. Chem.*, 1979, **83**, 241.
18 B. Gillot, *J. Solid State Chem.*, 1994, **113**, 163.
19 B. Gillot, M. Laarj, S. Kacim, T. Battault, R. Legros and A. Rousset, *Solid State Ionics*, 1996, **83**, 215.
20 R. Bendaoud, Ph. Tailhades, A. R. Fert, D. Bertrand, J. P. Redoulès and A. Rousset, *IEEE Trans. Magn.*, 1987, **23**, 3869.
21 B. Gillot, A. Rousset and G. Dupré, *J. Solid State Chem.*, 1978, **25**, 263.
22 B. Gillot, *Vibr. Spectrosc.*, 1994, **6**, 127.
23 M. Ishii, M. Nakahira and T. Yamanaka, *Solid State Commun.*, 1972, **11**, 209.
24 K. Siratori, *J. Phys. Soc. Jpn.*, 1967, **23**, 948.
25 B. Gillot, M. El Guendouzi and M. Kharroubi, *Mater. Chem. Phys.*, 1989, **24**, 199.
26 K. Terayama and M. Ikeda, *Trans. Jpn. Inst. Met.*, 1983, **24**, 754.
27 M. El Guendouzi and B. Gillot, *Mater. Chem. Phys.*, 1985, **13**, 179.
28 P. Barret, *Cinétique Hétérogène*, Gauthier-Villard, Paris, 1973.
29 B. Gillot, D. Delafosse and P. Barret, *Mater. Res. Bull.*, 1973, **8**, 1431.
30 K. L. Mampel, *Z. Phys. Chem. A*, 1940, **187**, 43.

Paper 6/07179A; *Received* 21*st October*, 1996